VIP Heterogeneous Catalysis

DOI: 10.1002/anie.201206152

Co/CoO Nanoparticles Assembled on Graphene for Electrochemical Reduction of Oxygen**

*Shaojun Guo, Sen Zhang, Liheng Wu, and Shouheng Sun**

The oxygen (O_2) reduction reaction (ORR) at/near ambient temperatures is an important cathodic reaction in polymer membrane electrolyte fuel cells (PEMFCs) and metal–air batteries (MABs).[1] Platinum has been the best metal found to catalyze the ORR. However, the use of Pt is costly, and in corrosive PEMFC and MAB reaction conditions, Pt-based catalysts tend to have very limited durability.[2–6] In searching for more robust and practical catalysts with comparative or even better catalytic performance than Pt, early transition metals supported on graphene (G) have attracted much attention. G is a single-layer, two-dimensional honeycomb-type carbon sheet that has large surface area, excellent conductivity, and good chemical stability.[7–9] It has been explored extensively either as nonmetal catalyst through molecular engineering[10–14] or as a unique support for metal catalysts.[15–18] Studies on G–metal interactions reveal that depending on the G–metal spacing and the Fermi level difference between G and the metal, there often exist a charge transfer across the G–metal interface.[19] Such a charge transfer may be the main reason why certain nanoparticles (NPs) supported on a G surface show enhanced catalytic activities, as demonstrated in the catalysts of G–Co_3O_4,[15] G–Fe_3O_4,[16] G–Co_xS_{1-x},[17] and G–$MnCo_2O_4$[18] for the ORR in alkaline[15,16,18] or acid[17] media. In these G–metal oxide catalyst systems, metal oxide NPs were deposited directly onto G surfaces through in situ chemical depositions.[15–18] Despite the fact that the depositions led to a tight G–NP contact, NPs prepared from these methods lacked the desired size and morphology control, thereby making it difficult to tune the G–NP interaction for better catalyst performance. Recently, we demonstrated a direct self-assembly method to deposit preformed monodisperse FePt NPs on a G surface,[19] and G–FePt showed much enhanced catalysis for the ORR in $HClO_4$ solution, thus indicating the G–NP interaction can indeed be tuned to enhance NP catalysis.

Herein we report that monodisperse Co/CoO NPs can be presynthesized and deposited on a G surface through the solution-phase self-assembly method, and the resulting G–Co/CoO is a high-performance electrocatalyst for the ORR in KOH (0.1M) solution. We demonstrate that their high catalytic performance originates not only from the G–Co/CoO interaction, but also from the dimension tuning of Co and CoO. The optimum G–Co/CoO NP catalyst with an 8 nm Co core and a 1 nm CoO shell is even better than the commercial Pt NP catalyst supported on carbon (C–Pt) concerning the ORR current density near the diffusion-limit current region, and this G–Co/CoO NP catalyst is more stable than the C–Pt catalyst.

G was produced by heating graphene oxide (GO) in dimethyl formamide (DMF) at 150 °C for six hours (see the Supporting Information).[19] Co NPs were synthesized through thermal decomposition of $[Co_2(CO)_8]$ in 1,2,3,4-tetrahydronaphthalene solution in the presence of oleic acid and dioctylamine (DOA, see the Supporting Information).[20] The Co-based NPs and G–Co/CoO NPs were characterized by transmission electron microscopy (TEM). Figure 1 A shows the typical TEM images of the as-prepared Co NPs. They are monodisperse 10 nm NPs with a narrow size distribution at ± 0.7 nm. When exposed to air at ambient condition, the top surface layers of Co were oxidized, thereby forming Co/CoO core/shell NPs. TEM analysis revealed that this CoO shell reached a thickness of approximately 1 nm (Figure 1 B and Figure S1 in the Supporting Information) and the thickness did not increase in nine days of continuous air exposure (Figure S2 in the Supporting Information), thus indicating that the CoO shell was able to protect Co from further oxidization in air at room temperature. However, Co in the Co/CoO NPs could be further oxidized when the NPs

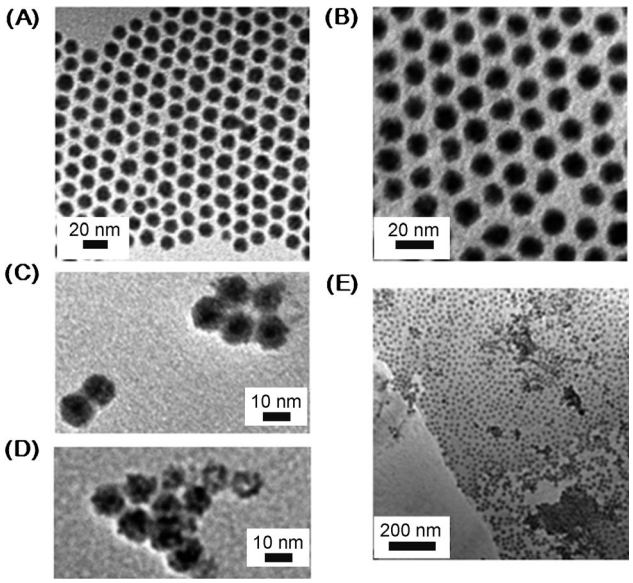

Figure 1. TEM images of Co NPs (A), Co/CoO core/shell NPs (B), Co/CoO NPs treated for 17 h (C) and 96 h (D) in air, and the Co/CoO core/shell NPs deposited on G surface (G–Co/CoO, E).

[*] Dr. S. Guo, S. Zhang, L. Wu, Prof. S. Sun
Department of Chemistry, Brown University
Providence, Rhode Island 02912 (USA)
E-mail: ssun@brown.edu

[**] Supported by the U.S. Department of Energy, Office of Energy Efficiency, and Renewable Energy, Fuel Cell Technologies Program.

Supporting information for this article is available on the WWW under http://dx.doi.org/10.1002/anie.201206152.

were heated at 70 °C in air. TEM images of the Co/CoO NPs heated at 70 °C for 17 and 96 h are shown in Figure 1 C, D. After heating for 17 h in air, the CoO layer grew to about 3 nm, while heating for 96 h led to higher-degree oxidation of Co, thereby giving a NP mixture of Co/CoO and hollow CoO NPs. When Co NPs were oxidized by an excess of trimethylamine *N*-oxide (Me_3NO) at 230 °C, hollow CoO NPs were obtained (Figure S3 in the Supporting Information). Here the hollow CoO NPs are formed through the nanoscale Kirkendall effect, which causes faster Co diffusion outwards than oxygen diffusion inwards.[21,22] All Co-based NPs could be assembled onto G by simply mixing the hexane dispersion of the NPs with a DMF solution of G under sonication (see the Experimental Section). Figure 1 E shows the typical TEM image of the Co/CoO NPs assembled on G. Similarly, the Co/CoO NPs were also deposited on Ketjen carbon (C) (C–Co/CoO). These C–Co/CoO NPs were used as a control to compare with G–Co/CoO NPs in the ORR studies.

X-ray diffraction (XRD) analyses indicate that the as-synthesized Co NPs have a multi-twinned *fcc* structure with the (111) peak appearing at $2\theta = 44.3°$ (Figure S4 in the Supporting Information). This structure is similar to what has been reported on Co NPs obtained from thermal decomposition of $[Co_2(CO)_8]$.[20] After Co NPs were transferred into hollow CoO NPs, new diffraction peaks at $2\theta = 36.7$, 42.7, and 62.1 °C, which belong to (111), (200), and (220) diffractions of the *fcc* CoO, were observed (Figure S4 in the Supporting Information). The Co/CoO NPs show typical Co and CoO dimension-dependent magnetization behavior, as shown in the room-temperature hysteresis loops of a series of Co/CoO NPs measured by vibrating sample magnetometer (VSM; Figure 2). The as-synthesized Co NPs show a superparamagnetic hysteresis loop with a saturation moment of 70.4 emu g^{-1} NPs (Figure 2 A). When Co NPs were exposed to air for five days, forming 8 nm/1 nm Co/CoO NPs, their moment was reduced to 40.4 emu g^{-1} NPs (Figure 2 B). Once further heated at 70 °C in air for 17 h and 96 h, the saturation moment of the resultant Co/CoO NPs was reduced to 24.2 and 16.2 emu g^{-1} (Figure 2 C, D). When the Co NPs were completely oxidized, the hollow CoO NPs were paramagnetic (Figure 2 E). Clearly, the moment reduction and magnetic property change was caused by the higher degree of Co oxidation in the Co/CoO structure.

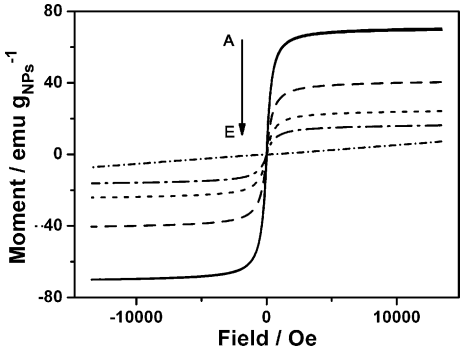

Figure 2. Room-temperature hysteresis loops measured by VSM of Co NPs (A), Co/CoO core/shell NPs (B), Co/CoO core/shell NPs heated at 70 °C in air for 17 h (C) and 96 h (D), and hollow CoO NPs (E, ×5 in moment).

The as-synthesized G–Co/CoO NPs and C–Co/CoO NPs were treated with butylamine (see the Experimental Section) to remove the original long-chain surfactant.[23] This room-temperature treatment was an important step to produce active Co/CoO catalysts. Figure S5 in the Supporting Information shows the typical ORR polarization curves of the C–Co/CoO NPs from different treatments. After washed with butylamine, the C–Co/CoO NPs exhibited a more positive half-wave potential for the ORR than those washed with ethanol under the same condition. Furthermore, energy dispersive X-ray (EDX) analysis on the Co/CoO NPs showed the reduced C/Co ratio after the butylamine treatment (Figure S6 in the Supporting Information). These results indicate that washing with butylamine was efficient to remove oleate/DOA. Figure 3 A shows the typical cyclic voltammograms (CVs) of oxygen reduction on the G-, C–Co/CoO-, and G–Co/CoO-modified glassy carbon (GC) electrodes in O_2-saturated KOH (0.1 M) solution with each catalyst having a mass loading of 20 μg. On the G-modified GC electrode, only a weak peak is seen at −0.360 V (vs. Ag/AgCl; Figure 3 A-i). When C–Co/CoO is present on the electrode, the peak becomes stronger and appears at −0.276 V (Figure 3 A-ii). Compared to G and the C–Co/CoO NPs, the G–Co/CoO NPs show a much stronger cathodic peak with the peak potential at −0.198 V (Figure 3 A-iii). These indicate that O_2 can be reduced much more easily on G–Co/CoO NPs than on G and C–Co/CoO NPs.

Rotating-disk electrode (RDE) measurements were further carried out to study ORR activity and kinetics on G, C–Co/CoO NPs, and G–Co/CoO NPs in the O_2-saturated KOH (0.1 M) solution. Figure 3 B shows the ORR polarization curves obtained at a rotation rate of 1600 rpm. The curve from G has a slow current increase and no current plateau (Figure 3 B-i), thus indicating that the ORR process on G is mainly a two-electron reduction of O_2 to OOH^-.[24] In contrast, ORR polarization curves from both C–Co/CoO and G–Co/CoO NPs have a sharp increase and reach quickly saturation (Figure 3 B-ii, iii). The G–Co/CoO NPs show a more positive half-wave potential (−0.176 V) for the ORR than the C–Co/CoO NPs (−0.290 V), thus indicating that G as a support indeed leads to a significant enhancement in Co/CoO catalysis for the ORR. RDE measurements also show that the limiting current density increases with increasing rotation rate (Figure 3 C). The corresponding Koutecky–Levich (K–L) plots show the inverse current density (j^{-1}) as a function of the inverse of the square root of the rotation speed ($\omega^{-1/2}$) at different potential values (Figure 3 D). The number of electrons involved per O_2 in the ORR on G–Co/CoO NPs were determined by the Koutecky–Levich equation:[25]

$$1/j = 1/j_k + 1/B\omega^{1/2} \quad (1)$$

where j_k is the kinetic current and ω is the electrode rotating rate. B is determined from the slope of the K–L plots based on the Levich equation:

$$B = 0.2nF(D_{O_2})^{2/3}\nu^{-1/6}C_{O_2} \quad (2)$$

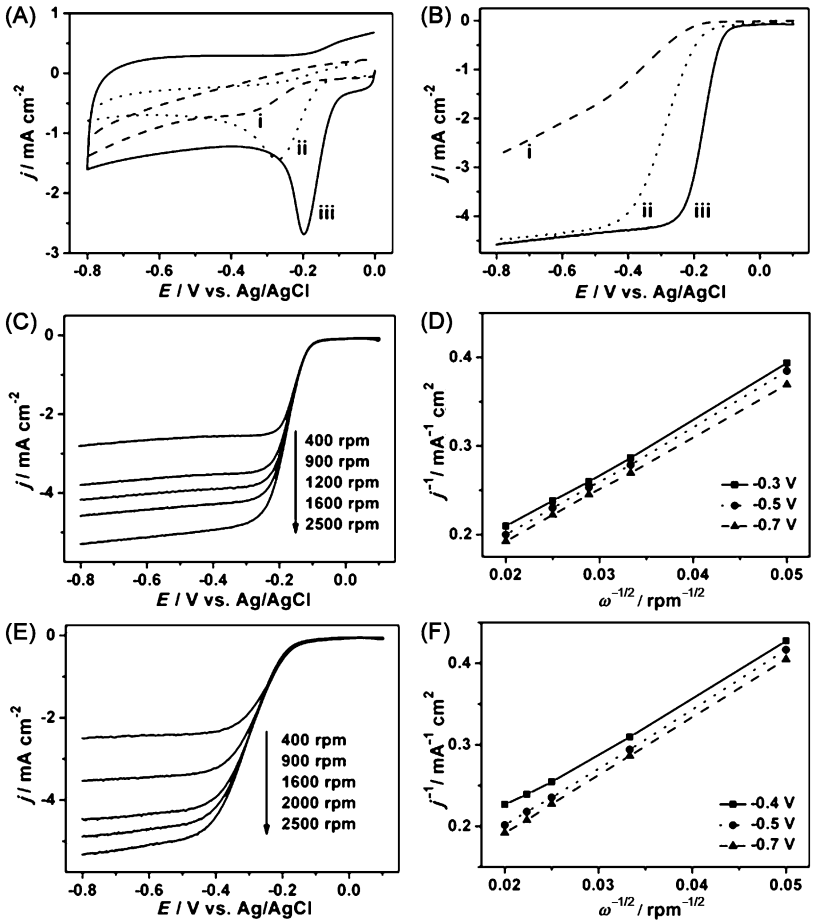

Figure 3. A, B) CVs (A) and ORR polarization curves (B) of GC electrodes modified with G (i), C–Co/CoO (ii), and G–Co/CoO (iii). (A): scan rate: 50 mV s^{-1}; (B): scan rate: 10 mV s^{-1} and rotation rate: 1600 rpm. C, E) ORR polarization curves of G–Co/CoO (C) and C–Co/CoO (E) at different rotation rates. D, F) K–L plots of the ORR from G–Co/CoO (D) and C–Co/CoO (F). The measurements were performed in O_2-saturated KOH (0.1 M) solution.

where n represents the number of electrons gained per O_2, F is the Faraday constant ($F = 96485$ C mol^{-1}), D_{O_2} is the diffusion coefficient of O_2 in 0.1 M KOH (1.9×10^{-5} cm^2 s^{-1}),[25b] ν is the kinetic viscosity (0.01 cm^2 s^{-1}), and C_{O_2} is the bulk concentration of O_2 (1.2×10^{-6} mol cm^{-3}). Figure 3D shows three linear K–L plots at different potentials, suggesting the first-order reaction kinetics toward the concentration of O_2 on G–Co/CoO NPs from −0.3 V to −0.7 V. n in Equation (2) can be calculated to be between 4.08–4.15, thereby indicating that the ORR from −0.3 V to −0.7 V is dominated by a four-electron (4e) process and O_2 is reduced to OH^-. Similarly, the ORR kinetics on the C–Co/CoO NPs can be analyzed (Figure 3E). The corresponding K–L plots (Figure 3F) give $n = 3.9$ at −0.5 V, thus revealing that the C–Co/CoO NPs still favor a 4e oxygen reduction process. Furthermore, compared to those from the C–Co/CoO NPs (Figure 3E), the ORR polarization curves from the G–Co/CoO NPs (Figure 3C) have steeper slopes in the kinetic region, thereby further confirming that the G–Co/CoO NPs are more favorable for oxygen reduction than the C–Co/CoO NPs.

When considering that the Co core in Co/CoO NPs may have an important role in enhancing the catalytic activity in the ORR, we further studied the activities of the G–Co/CoO NPs with different CoO thicknesses under the same condition (Figure 4A). With the increased CoO coating from 1 to 3 nm and even thicker, the G–Co/CoO NPs exhibited negative polarization shifts, thus indicating that the thin CoO shell facilitates the oxygen reduction. We should note that although the G–Co/CoO NPs with a thick CoO shell have a lower half-wave potential for the ORR, they can still catalyze the ORR through a 4e process (Figures S7 and S8 in the Supporting Information).

The ORR catalytic activity of the G–Co/CoO NPs was compared with that of the commercial C–Pt catalyst in the O_2-saturated KOH (0.1 M) solution. The half-wave potential difference between G–Co/CoO and C–Pt is 25 mV under the same condition (Figure 4B). However, the G–Co/CoO NPs have a steeper polarization curve and a higher current density than the C–Pt catalyst from −0.185 V to −0.6 V, thereby indicating that G–Co/CoO and C–Pt have a comparative activity in the ORR. The durability of the G–Co/CoO NPs and C–Pt was

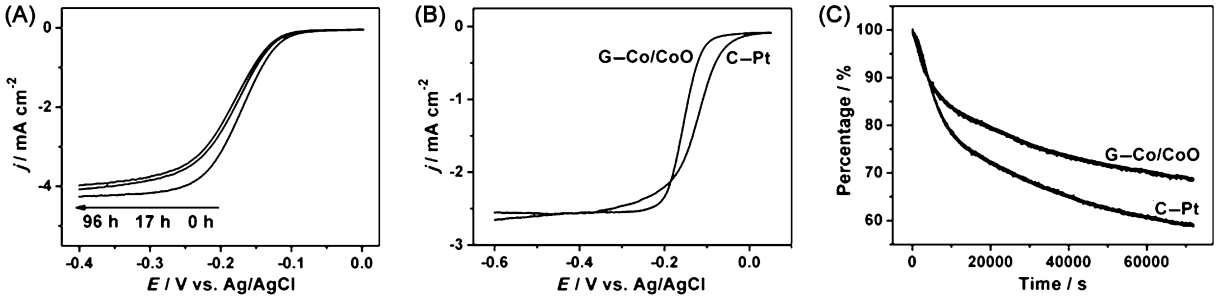

Figure 4. A) ORR polarization curves of G–Co/CoO NPs heated at 70 °C in air for 0 h, 17 h, and 96 h. B) ORR polarization curves of the G–Co/CoO NPs and commercial C–Pt catalyst. Scan rate: 10 mV s^{-1} in (A) and (B), and rotation rate: 1600 rpm in (A) and 400 rpm in (B). C) The chronoamperometric responses for the ORR on the G–Co/CoO NPs and commercial C–Pt catalyst at −0.3 V. Rotation rate: 200 rpm. The measurements were performed in O_2-saturated KOH (0.1 M) solution.

also evaluated by using a chronoamperometric method at −0.3 V (Figure 4C). The current densities from both G–Co/CoO and C–Pt decrease with time in the same pace initially. But G–Co/CoO shows a slower decrease than C–Pt after 20 h stability test, demonstrating a longer-term stability of the G–Co/CoO over the C–Pt/catalyst. A similar study indicates that G–Co/CoO is also more stable than C–Co/CoO (Figure S9 in the Supporting Information). These results prove that G can activate and stabilize Co/CoO NPs more efficiently for the ORR and the present G–Co/CoO NPs are a promising alternative to the C–Pt catalyst in KOH.

In summary, the G–Co/CoO NPs have been synthesized by self-assembly of Co NPs onto the surface of G. The Co NPs tend to form a layer (ca. 1 nm) of natural CoO once they are exposed to ambient environment. This CoO layer prevents Co from deep oxidation unless the Co/CoO NPs(1 nm shell) are heated at an elevated temperature (70 °C). With this controlled oxidation, we have obtained a series of G–Co/CoO NPs with tunable Co size and CoO thickness. Co in Co/CoO NPs can be completely oxidized by an excess of Me_3NO, thereby forming hollow CoO NPs. Compared to G and C–Co/CoO NPs, the G–Co/CoO NPs show much enhanced catalytic activity for the ORR in O_2-saturated KOH (0.1M) solution, and their activity depends on the CoO thickness; the G–Co/CoO NPs with a 1 nm CoO shell show the maximum activity. The work demonstrates the importance of Co/CoO dimension and G as a support in tuning electrocatalysis for efficient ORR. The optimized G–Co/CoO NPs have a comparative activity and better stability than the commercial C–Pt NPs and may serve as a promising alternative to C–Pt catalysts for the ORR in alkaline solutions.

Experimental Section

Synthesis of G-Co/CoO and C-Co/CoO: Co NPs (60 mg, synthetic details are given in the Supporting Information) dispersed in hexane (60 mL) were added into a DMF solution (60 mL) of G (1 mg mL^{-1}) under sonication, and the mixture was further sonicated for one hour. Similarly, Co NPs (60 mg) were also deposited on Ketjen carbon (60 mg) by sonication to make C–Co/CoO NPs.[26] After ethanol (120 mL) was added, the precipitate was separated from the solvents by centrifuging for ten minutes at 9500 rpm. The as-obtained NP catalyst was dispersed in butylamine (60 mL) through sonication, and further stirred for three days at ambient temperature.[23] After ethanol (60 mL) was further added into the above butylamine solution, the catalyst was centrifuged at 9000 rpm for ten minutes. After that, the catalyst was further dried and divided into several parts. Two parts of catalysts were heated at 70 °C in air for 17 h and 96 h to get G–Co/CoO core/shell NPs with different shell thickness.

Catalyst preparation and deposition on the working electrode: The NP catalyst was redispersed in a mixture of solvents containing water, isopropanol, and Nafion (5%) (v/v/v = 4:1:0.025) to form a 2 mg mL^{-1} suspension. The GC working electrode was first polished with 1.0 and 0.05 μm alumina powder, rinsed with deionized water, and sonicated first in ethanol and then in double-distilled water. The catalyst ink (10 μL) was casted on the electrode and dried at ambient condition. CVs of different catalysts were carried out in a KOH (0.1M) solution at a scan rate of 50 mV s^{-1}. The RDE measurements of different catalysts were conducted in O_2-saturated KOH (0.1M) solution at the scan rate of 10 mV s^{-1} and different rotation rates.

Characterization: TEM images were acquired on a Philips CM 20 EM microscope operating at 200 kV. X-ray diffraction (XRD) characterization was carried out on a Bruker AXS D8-Advanced diffractometer with Cu Kα radiation ($\lambda = 1.5418$ Å). HRTEM image was obtained on a JEOL 2010 with an accelerating voltage of 200 kV. Magnetic studies were carried out using a Lakeshore 7404 high-sensitivity vibrating sample magnetometer (VSM) with fields up to 1.5 T. The electrochemical measurements were performed on a potentiostat (Autolab 302) with Ag/AgCl (vs. 4M KCl) as a reference electrode and Pt wire as a counter electrode.

Received: August 1, 2012
Published online: October 16, 2012

Keywords: cobalt · graphene · heterogeneous catalysis · nanoparticles · oxygen reduction

[1] Y. Bing, H. Liu, L. Zhang, D. Ghosh, J. Zhang, *Chem. Soc. Rev.* **2010**, *39*, 2184 – 2202.
[2] Z. Peng, H. Yang, *J. Am. Chem. Soc.* **2009**, *131*, 7542 – 7543.
[3] M.-H. Shao, K. Sasaki, R. R. Adzic, *J. Am. Chem. Soc.* **2006**, *128*, 3526 – 3527.
[4] V. R. Stamenkovic, B. Fowler, B. S. Mun, G. J. Wang, P. N. Ross, C. A. Lucas, N. M. Markovic, *Science* **2007**, *315*, 493 – 497.
[5] S. Guo, E. Wang, *Nano Today* **2011**, *6*, 240 – 264.
[6] G. Wu, K. L. More, C. M. Johnston, P. Zelenay, *Science* **2011**, *332*, 443 – 447.
[7] S. Guo, S. Dong, *Chem. Soc. Rev.* **2011**, *40*, 2644 – 2672.
[8] S. Guo, S. Dong, E. Wang, *ACS Nano* **2010**, *4*, 547 – 555.
[9] S. Guo, D. Wen, S. Dong, E. Wang, *ACS Nano* **2010**, *4*, 3959 – 3968.
[10] Y. Li, Y. Zhao, H. Cheng, Y. Hu, G. Shi, L. Dai, L. Qu, *J. Am. Chem. Soc.* **2012**, *134*, 15 – 18.
[11] L. Qu, Y. Liu, J.-B. Baek, L. Dai, *ACS Nano* **2010**, *4*, 1321 – 1326.
[12] Z.-H. Sheng, L. Shao, J.-J. Chen, W.-J. Bao, F.-B. Wang, X.-H. Xia, *ACS Nano* **2011**, *5*, 4350 – 4358.
[13] Z. Yao, H. Nie, Z. Yang, X. Zhou, Z. Liu, S. Huang, *Chem. Commun.* **2012**, *48*, 1027 – 1029.
[14] Y. Li, W. Zhou, H. Wang, L. Xie, Y. Liang, F. Wei, J.-C. Idrobo, S. J. Pennycook, H. Dai, *Nat. Nanotechnol.* **2012**, *7*, 394 – 400.
[15] Y. Liang, Y. Li, H. Wang, J. Zhou, J. Wang, T. Regier, H. Dai, *Nat. Mater.* **2011**, *10*, 780 – 786.
[16] Z.-S. Wu, S. Yang, Y. Sun, K. Parvez, X. Feng, K. Müllen, *J. Am. Chem. Soc.* **2012**, *134*, 9082 – 9085.
[17] H. Wang, Y. Liang, Y. Li, H. Dai, *Angew. Chem.* **2011**, *123*, 11161 – 11164; *Angew. Chem. Int. Ed.* **2011**, *50*, 10969 – 10972.
[18] Y. Liang, H. Wang, J. Zhou, Y. Li, J. Wang, T. Z. Regier, H. Dai, *J. Am. Chem. Soc.* **2012**, *134*, 3517 – 3523.
[19] S. Guo, S. Sun, *J. Am. Chem. Soc.* **2012**, *134*, 2492 – 2495.
[20] S. Peng, J. Xie, S. Sun, *J. Solid State Chem.* **2008**, *181*, 1560 – 1564.
[21] S. Peng, S. Sun, *Angew. Chem.* **2007**, *119*, 4233 – 4236; *Angew. Chem. Int. Ed.* **2007**, *46*, 4155 – 4158.
[22] Y. Yin, R. M. Rioux, C. K. Erdonmez, S. Hughes, G. A. Somorjai, A. P. Alivisatos, *Science* **2004**, *304*, 711 – 714.
[23] J. Wu, J. Zhang, Z. Peng, S. Yang, F. T. Wagner, H. Yang, *J. Am. Chem. Soc.* **2010**, *132*, 4984 – 4985.
[24] Y. Zheng, Y. Jiao, J. Chen, J. Liu, J. Liang, A. Du, W. Zhang, Z. Zhu, S. C. Smith, M. Jaroniec, G. Q. Lu, S. Z. Qiao, *J. Am. Chem. Soc.* **2011**, *133*, 20116 – 20119.
[25] a) S. Wang, D. Yu, L. Dai, *J. Am. Chem. Soc.* **2011**, *133*, 5182 – 5185; b) S. Wang, D. Yu, L. Dai, D. W. Chang, J.-B. Baek, *ACS Nano* **2011**, *5*, 6202 – 6209; c) S. Wang, E. Iyyamperumal, A. Roy, Y. Xue, D. Yu, L. Dai, *Angew. Chem.* **2011**, *123*, 11960 – 11964; *Angew. Chem. Int. Ed.* **2011**, *50*, 11756 – 11760; d) K. Gong, F. Du, Z. Xia, M. Durstock, L. Dai, *Science* **2009**, *323*, 760 – 764.
[26] a) V. Mazumder, S. Sun, *J. Am. Chem. Soc.* **2009**, *131*, 4588 – 4589; b) S. Guo, S. Zhang, X. Sun, S. Sun, *J. Am. Chem. Soc.* **2011**, *133*, 15354 – 15357.

